RESEARCH PAPER

PCCP
www.rsc.org/pccp

The nature of water on surfaces of laboratory systems and implications for heterogeneous chemistry in the troposphere

Ann Louise Sumner,[a] Erik J. Menke,[b] Yael Dubowski,[b] John T. Newberg,[b] Reginald M. Penner,[b] John C. Hemminger,[b] Lisa M. Wingen,[b] Theo Brauers[c] and Barbara J. Finlayson-Pitts*[b]

[a] *Battelle, 505 King Ave., Columbus, OH 43201-2693, USA*
[b] *Department of Chemistry, University of California, Irvine, Irvine, CA 92697-2025, USA. E-mail: bjfinlay@uci.edu; Fax: +1 (949) 824-3168; Tel: +1 (949) 824-7670*
[c] *Institut für Atmosphärische Chemie (ICG3), Forschungszentrum KFA Jülich, D-52425 Jülich, Germany*

Received 17th July 2003, Accepted 8th December 2003
First published as an Advance Article on the web 12th January 2004

A number of heterogeneous reactions of atmospheric importance occur in thin water films on surfaces in the earth's boundary layer. It is therefore important to understand the interaction of water with various materials, both those used to study heterogeneous chemistry in laboratory systems, as well as those found in the atmosphere. We report here studies at 22 °C to characterize the interaction of water with such materials as a function of relative humidity from 0–100%. The surfaces studied include borosilicate glass, both untreated and after cleaning by three different methods (water, hydrogen peroxide and an argon plasma discharge), quartz, FEP Teflon film, a self assembled monolayer of *n*-octyltrichlorosilane (C8 SAM) on glass, halocarbon wax coatings prepared by two different methods, and several different types of Teflon coatings on solid substrates. Four types of measurements covering the range from the macroscopic level to the molecular scale were made: (1) contact angle measurements of water droplets on these surfaces to obtain macroscopic scale data on the water-surface interaction, (2) atomic force microscopy measurements to provide micron to sub-micron level data on the surface topography, (3) transmission FTIR of the surfaces in the presence of increasing water vapor concentrations to probe the interaction with the surface at a molecular level, and (4) X-ray photoelectron spectroscopy measurements of the elemental surface composition of the glass and quartz samples. Both borosilicate glass and the halocarbon wax coatings adsorbed significantly more water than the FEP Teflon film, which can be explained by a combination of the chemical nature of the surfaces and their physical topography. The C8 SAM, which is both hydrophobic and has a low surface roughness, takes up little water. The implications for the formation of thin water films on various surfaces in contact with the atmosphere, including building materials, soil, and vegetation, are discussed.

I. Introduction

Heterogeneous processes in the troposphere have a substantial impact on trace gas concentrations. For example, a number of heterogeneous reactions, including the nitrogen dioxide hydrolysis reaction (1) and the reaction (2) of adsorbed nitric acid with gaseous nitric oxide,

$$2NO_2 + H_2O \xrightarrow{\text{surface}} HONO + HNO_3 \qquad (1)$$

$$2NO + HNO_3 \xrightarrow{\text{surface}} HONO + NO_3 \qquad (2)$$

occur in thin water films present on surfaces. Such reactions have been observed to depend on the water vapor concentration,[1–5] which is reasonable since the relative humidity (RH) determines the equilibrium concentration of water on the surface.

The formation of nitrous acid in reaction (1) has been particularly well-studied in many different laboratories using a variety of reactors, surface materials, and coatings.[2–22] HONO is a major source of the hydroxyl radical (OH) in polluted urban regions,[23–29] which drives the chemistry of both remote and urban atmospheres. Since subsequent oxidation of organic compounds by OH radicals and other oxidants in the presence of nitrogen oxides and sunlight produce ozone as well as other secondary pollutants in the troposphere,[30] understanding the sources and sinks of HONO is critical for accurately modeling the troposphere and predicting future trace gas concentrations.

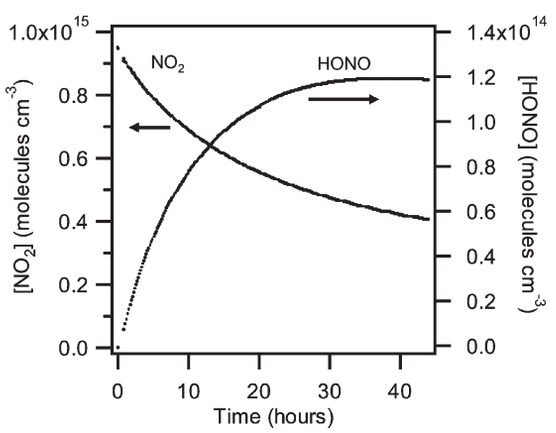

Fig. 1 Loss of NO_2 and formation of HONO at 24 °C from the heterogeneous hydrolysis of NO_2 on the surface of a 561 L chamber coated with halocarbon wax using the dip method. Measurements were made using differential optical absorption spectrometry (DOAS). Initial concentration of NO_2 was 38.6 ppm and the RH was 85%.

DOI: 10.1039/b308125g

Fig. 1 shows an example of a study of reaction (1) carried out in this laboratory at 85% RH and 24 °C in a 561 L chamber, described previously,[31] whose internal surfaces were coated with hydrophobic halocarbon wax. This coating is often used in laboratory studies as it is chemically inert, like Teflon, but can be easily applied and removed. Despite the fact that only small amounts of water would be expected on such a hydrophobic surface, loss of NO_2 and formation of HONO does indeed occur. Furthermore, when corrected to a common reaction chamber surface-to-volume ratio (S/V) and to an RH of 50%, the rate of HONO formation (4.5×10^{-2} ppb min^{-1} per ppm NO_2) is in good agreement with rates measured in larger (5800 L) Teflon-coated smog chambers (3.9×10^{-2} ppb min^{-1} per ppm NO_2),[2] and in smaller (7–19 L) borosilicate glass cells [$(2–4) \times 10^{-2}$ ppb min^{-1} per ppm NO_2].[5] This agreement is remarkable, given the very different nature of the chamber materials ranging from hydrophobic (Teflon, halocarbon wax) to hydrophilic (glass), for which different amounts of water might be expected to be available on the surface for reaction.

A prerequisite to fully understanding such heterogeneous processes is understanding the amount and nature of water on the surfaces. The goal of this work is therefore to elucidate the interaction of water at room temperature with some surfaces typically used in laboratory systems, and related materials, that can provide insight into the role of these thin films in atmospheric reactions. The materials studied include the following: (1) borosilicate glass as provided by the manufacturer; (2) borosilicate glass cleaned using water, hot H_2O_2, or an argon plasma discharge; (3) quartz; (4) thin FEP Teflon film; (5) halocarbon wax-coated glass using two different coating methods; (6) glass coated with a C8 organic self-assembled monolayer (SAM); and (7) several thick Teflon coatings applied to solid substrates. Four different types of measurements were made that provide insights from the macroscopic to molecular level. On a macroscopic scale, contact angle measurements of water droplets on these surfaces were obtained to examine the wettability of the surfaces. On a micron to sub-micron scale, atomic force microscopy (AFM) measurements provide insight into the surface structure. On the molecular level, transmission FTIR of the surfaces in the presence of increasing water vapor concentrations was used to probe the nature and amounts of water on the surfaces. Finally, X-ray photoelectron spectroscopy (XPS) was used to study the elemental surface composition of the glass and quartz samples for which water uptake measurements were made. The implications for understanding heterogeneous reactions in or on surface water films in laboratory systems as well as extrapolation to atmospheric surfaces are discussed.

II. Experimental methods

A. Surface materials

The materials included in this study, many of which are commonly used in laboratory experiments, are summarized in Table 1. They include both hydrophilic and hydrophobic materials. The hydrophilic materials are thin cover slips of smooth glass (VWR Micro Cover Glasses) and quartz (Quartz Plus, Inc.). Cover glass discs were used because they were sufficiently thin that they did not significantly attenuate the infrared beam in the region of interest (above 2000 cm^{-1}). Standard borosilicate laboratory glass (Type I, Class A)[32] used in many laboratory studies of heterogeneous reactions has a higher silica content, but like the cover slips, also contains small amounts of boron, sodium and aluminum oxides (see Table 1). The overall similarity between the Type I, Class A glass and the cover slips is such that using the latter to probe interactions with water is reasonable.

Measurements were conducted on the hydrophilic glass as received from the manufacturer, and also after employing three different treatments. In the first case, the glass discs were rinsed with Nanopure water (Barnstead, 18.1 MΩ cm) and dried in nitrogen (Oxygen Service Co., ≥99.999%). In the second case, the discs were cleaned for 35 minutes with an argon plasma discharge (Harrick Scientific Plasma Cleaner/Sterilizer PDC-32G, medium power). For the third treatment, which has been suggested for cleaning porous glass surfaces,[33] the discs were submerged in hot (~85 °C) H_2O_2 (30%, Electron Microscopy Sciences, ACS Reagent Grade) for approximately 10 minutes, followed by thorough rinsing with Nanopure water and drying in the cell in a stream of dry nitrogen gas at 40 °C overnight.

A variety of hydrophobic materials were also analyzed for their water uptake characteristics. Halocarbon wax (Halocarbon Products Corp., Series 1500) samples were prepared in two ways, each utilizing the smooth glass discs as the substrate. For the "dip method," the glass discs were dipped into melted halocarbon wax and mounted in the sample holder. The coated discs were then gently warmed with a heat gun until the wax appeared to flow freely to reduce the impact of air bubbles on the surface. The coated discs were cloudy to the eye but appeared to have a smooth and quite thick coating. The "solvent method" involved submerging the glass discs in a warm solution of halocarbon wax dissolved in

Table 1 Samples used for water uptake measurements and surface characterization

Material	Description	Chemical composition	Source
Smooth glass	Micro cover glasses, No. 1, 25 mm dia. × 0.13–0.17 mm	64% SiO_2, 9% B_2O_3, 7% ZnO, 7% K_2O, 7% Na_2O, 3% TiO_2, 3% Al_2O_3	VWR Scientific, Inc., Buffalo Grove, IL
Laboratory glass[a]	Designation E438-92: specification for Type I, Class A[32]	81% SiO_2, 13% B_2O_3, 4% Na_2O, 2% Al_2O_3	ASTM International West Conshohocken, PA
Quartz	Quartz cover slips substrate grade, 25 mm dia. × 0.16 mm	Corning 7980 Synthetic Fused Silica: > 99.9% SiO_2	Quartz Plus, Inc. Brookline, NH
Halocarbon wax	Series 1500	Polychlorotrifluoroethylene	Halocarbon Products Corp. River Edge, NJ
FEP film	2 mil FEP Teflon film	Fluoropolymer	Norton Performance Plastics
Organic SAM	C8 self assembled monolayer	*n*-octyltrichlorosilane: 95%	Geselt
FEP coating	FEP Teflon coating CCI-109	Fluoropolymer	Crest Coating Inc. Anaheim, CA
PFA coating	PFA Teflon coating	Fluoropolymer	Crest Coating, Inc. Anaheim, CA
Fluoropolymer coating	FluoroPel PFC801A	Fluoropolymer	Cytonix Corp. Beltsville, MD

[a] Data provided for comparison.

dichloromethane (EM Science, 99.8%). The samples were also gently heated with a heat gun. The resulting coating was hazy to the eye, but obviously much thinner than the coating using the dip method.

Samples of thin FEP Teflon film (Norton High Performance Films) were supported by thin halocarbon wax-coated aluminum washers for the infrared study. The Teflon film was pressed onto the warm halocarbon wax coating, which held the film firmly in place, and the excess film removed.

Self-assembled monolayers of *n*-octyltrichlorosilane (Geselt, 95%) were deposited on borosilicate glass discs according to a well-established technique.[34] Briefly, the glass discs were cleaned with boiling ethanol, then with boiling chloroform. The dry glass was further cleaned with an argon plasma discharge for ~30 minutes. Upon removal from the plasma cleaner, the substrates were stored in Nanopure water until deposition of the monolayer was carried out. After drying the surfaces with nitrogen, the discs were placed in a mM solution of *n*-octyltrichlorosilane in dodecane for 10 min. The C8 SAM-coated discs were then placed in boiling chloroform to remove any physisorbed material. The coating and chloroform extraction steps were repeated two additional times to ensure a smooth, well-ordered coating.

Three additional hydrophobic materials, two Teflon spray-coated materials and a fluoropolymer coating, were also studied. Such coatings are commonly used in laboratory systems, such as in smog chambers,[2,12] in which many studies of atmospheric reactions have been carried out. Due to the substrate material (metal and thick glass), these materials could not be probed by infrared spectroscopy. However, analysis of the wetting and surface characteristics could still be studied as described in sections II B and C, respectively. The Teflon spray-coated materials, Teflon FEP CCI-109 and PFA Teflon, were used as received from the manufacturer. The third material, a fluoropolymer coating, was applied as a 1% FluoroPel PFC 801A emulsion in a fluoropolymer to a glass microscope slide.[35] The coating was then annealed at 90 °C and the solvent evaporated.

B. Water contact angle

Surface wettability of the materials described above was probed by contact angle measurements using water droplets. Quasi-equilibrium contact angles of sessile 1 μl Nanopure water droplets were measured under ambient conditions with a Kodak DCS 315 camera equipped with a long-range microscope (Infinity Optics). The shape of the droplet depends on its interaction with the surface.[36] The line tangent to the curve of the droplet to the point where it intersects the solid surface forms the contact angle. A water droplet resting on a hydrophobic surface would form a spherical droplet having a high contact angle, but would have a much smaller contact angle when placed on a more hydrophilic surface.

C. Surface characterization

Atomic force microscopy (AFM) was used to probe the physical topography of the air/solid interface of the samples described above. Samples were imaged with a Park Scientific Instruments (PSI) Autoprobe LS Atomic Force Microscope under ambient conditions. The images were obtained in either contact mode with PSI Ultralever B tips, with the tip force set to approximately 25 nN, or in non-contact mode with PSI Ultralever C tips. In contact mode, each 256×256 pixel image took approximately 5 min to obtain, with a scan rate of 1 Hz in the fast (horizontal) direction. In non-contact mode, each 256×256 pixel image took approximately 10 min, with a scan rate of 0.5 Hz. RMS roughness values were calculated using the PSI ProScan software on background corrected AFM images. Background correction involved the fitting of each scan line in an AFM image with a second order polynomial, and the subtraction of this best fit curve from the raw data. This procedure left intact all surface roughness on a length scale smaller than one-half the image size, but it removed lower frequency noise and the tube curvature artifact from the data. No Fourier filtering of AFM images was carried out.

D. Water uptake measurements

The amount of liquid water adsorbed on the surfaces was determined as a function of relative humidity by transmission Fourier transform infrared spectroscopy (FTIR). The samples of interest were positioned within a glass cell enclosed with 32 mm diameter ZnSe windows, as shown in Fig. 2. The cell had an 11 cm path length and could accommodate thin, disc-shaped, samples with a diameter up to 2.5 cm. The center O-ring permitted installation and removal of the samples, which were positioned an average of ~6 mm apart in thin slots cut in a glass holder and secured with small amounts of halocarbon wax. Up to ten samples could be mounted in the cell, allowing for the measurement of water uptake on a total of 20 surfaces. All gas flows through the cell were set using calibrated flow meters (Matheson TF 1050). A type-K thermocouple with an Omega HH202A digital readout (±0.25% reading +0.2 °C) was positioned inside the cell to monitor the cell temperature during experiments. All measurements were conducted at atmospheric pressure under dynamic conditions with a total flow rate of 200 mL min^{-1}.

The relative humidity in the cell was set by mixing flows of dry and 100% RH nitrogen, obtained by passing N_2 through Nanopure water in two borosilicate glass fritted bubblers, in series. The bubblers were kept in a water bath set at 22.0 ± 0.2 °C (MGW Lauda MT) to reduce the effects of evaporative cooling. The temperature of the cell in the FTIR sample compartment, which was normally ~3 °C warmer than the room, was cooled by passing the spectrometer purge gas (25 L min^{-1} flow rate) through a stainless steel coil in a temperature controlled bath (MGW Lauda RCS) set at −8 °C. Heat tape was wrapped around the glass cell and used to fine-tune the cell temperature, which was maintained at 22.0 ± 0.2 °C. The use of Teflon tubing was minimized in favor of non-porous materials including glass and stainless steel. This was intended to reduce the degassing of water vapor from within the porous Teflon walls and also the permeation of room air through the tubing. The KBr windows separating the spectrometer's sample and interferometer/detector compartments were removed; even under fast dry nitrogen purge, the KBr windows held variable amounts of liquid water, which generated an irreproducible signal that was often significant compared to the water adsorbed on the samples of interest.

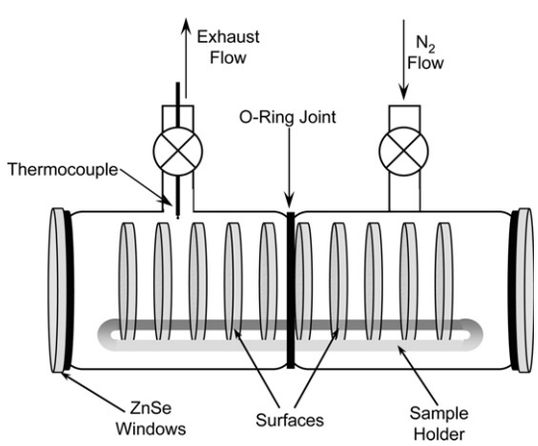

Fig. 2 Cell used for measurements of water uptake on glass and other surfaces.

Spectra of the glass and other materials in equilibrium with humidified N_2 were obtained as interferograms at 1 cm^{-1} resolution on an FTIR spectrometer (Mattson, Galaxy 5020) equipped with a liquid nitrogen cooled mercury cadmium telluride detector. The samples were dried in the cell overnight under a flow of dry N_2 (200 mL min^{-1}) at 40 °C. To ensure that the nitrogen was completely dry, the vapor above liquid N_2 (Airgas, 55 psi) was used. After cooling the cell to 22 °C, a background spectrum of 2048 scans was obtained each day, with a flow of dry nitrogen through the cell. The dry and humid nitrogen flows were then set to the desired relative humidity and flow through the cell was established. Sample spectra of 1024 scans were obtained at each relative humidity after an equilibration time of 15 min.

Water vapor spectra for subtraction were also measured with the samples removed from the glass cell. During water vapor spectra collection, an optical filter was used to remove IR radiation below 2000 cm^{-1}. Infrared radiation was reflected off the cell windows and returned to the interferometer where it was remodulated and its phase shifted by 180°. This phenomenon has been described by Griffiths and de Haseth[37] and was observed in this system as negative peaks in the 3200 cm^{-1} region; the peaks resulted from the water bend in the 1600 cm^{-1} region that were frequency-doubled upon remodulation. The optical filter was constructed from three borosilicate glass discs (described above) that were held together with halocarbon wax. The outer surfaces were covered with FEP Teflon film to minimize water uptake on the filter. The FEP film was roughened with 1 μm diamond polishing paper to eliminate multiple reflections within the film, as described below. The optical filter efficiently absorbed the IR radiation at wavenumbers below 2000 cm^{-1} that had caused the interference. Any small amounts of liquid water that may have been present on the ZnSe windows or the optical filter were subtracted from the sample spectra, along with water vapor.

A problem that often arises with the use of thin parallel surfaces in transmission IR spectroscopy is multiple reflection of the IR radiation between the two surfaces.[37] The multiple reflections cause interference fringes on either side of the centerburst in the interferograms and result in sinusoidal noise peaks in the single beam and absorbance spectra. Replacing these fringes in the interferogram with zeros before the Fourier transform is performed has the effect of removing the interference pattern from the single beam spectrum.[37] While this zero-filling procedure adds small amounts of noise to the spectrum, the final result is much more useful. Thus, interference fringes were typically removed from the interferogram before performing the Fourier transform, for which 5064 interferogram data points were used to calculate 4 cm^{-1} resolution single beam spectra. Absorbance spectra were obtained by ratioing the single beam spectrum for a given relative humidity to the background spectrum from that day. Although the noise that resulted from the internal reflections in the quartz samples was apparent in the single beam spectra, it was not visible in the ratioed absorbance spectra. Interference fringes were not produced for the halocarbon wax dip method samples whose surfaces were not smooth, and hence did not have interference from multiple internal reflections.

E. X-ray photoelectron spectroscopy

X-ray photoelectron spectroscopy (XPS) was used to probe the elemental composition of the air/solid interface of the glass (both untreated and cleaned/treated) and quartz samples to provide insight into the changes induced by each treatment technique. X-ray photoelectron spectra of the surfaces were obtained in an ESCALAB MKII ultra-high vacuum (UHV) instrument (VG Scientific) equipped with three individually pumped chambers, allowing for rapid transfer (<1 h) of samples from atmospheric to UHV pressures. Sample surfaces were irradiated under UHV ($\sim 5 \times 10^{-10}$ Torr) with 1486.6 eV X-rays from an aluminum anode at 15 keV and 20 mA. The kinetic energies of the ejected photoelectrons were analyzed using a 150 mm hemispherical electron energy analyzer. Data collection and analysis were carried out using the software package PISCES (Dayta Systems Ltd.). XPS peak areas were integrated after a linear background subtraction. The surface concentrations were determined by dividing the integrated areas by standard sensitivity factors (relative to an F(1s) sensitivity factor of 1.0).[38,39] The sensitivity factors used are as follows: O(1s), 0.721; Si(2p), 0.355; C(1s), 0.306; B(1s), 0.165; Zn($2p_{3/2}$), 3.734; K($2p_{3/2}$), 1.013; Na(1s), 1.655; Ti($2p_{3/2}$), 1.360; Al(2p), 0.246. Due to the uncertainty in the sampling depth for each element, the surface composition should be considered semi-quantitative.

III. Results

A. Contact angles for the surfaces with water

Interaction of water with the surfaces studied here on a macroscopic scale can be characterized by the contact angle. Fig. 3 shows the results of three typical contact angle measurements made for a hydrophobic surface (halocarbon wax, Fig. 3a), a hydrophilic surface (plasma-cleaned borosilicate glass, Fig. 3c) and an intermediate surface (untreated borosilicate glass, Fig. 3b). As expected, the contact angle is large for the hydrophobic surface and small for the hydrophilic surface. The intermediate contact angle measured for the untreated borosilicate glass is indicative of organic contamination on the surface, as supported by XPS measurements discussed below.

Table 2 summarizes the measured contact angles for the various materials. They can be grouped into three categories: (1) high contact angles (>80°) measured for the halocarbon wax, Teflon coatings and a C8 SAM on solid substrates, (2) low contact angles (<10°) exemplified by the cleaned borosilicate glass, and (3) intermediate values represented by the untreated borosilicate glass, the water-rinsed glass and quartz.

B. AFM measurements of the surface morphology

Figs. 4 and 5 show typical AFM images of representative surfaces. For each sample the root mean square (RMS) surface roughness was calculated as follows:

$$R_{\mathrm{RMS}} = \sqrt{\frac{\sum_{n=1}^{N} (z_n - \bar{z})^2}{N-1}} \qquad \text{(I)}$$

where $\bar{z}$ is the average z height and N is the number of points sampled. However, it should be noted that these are minimum values since, in many cases, the pores on the surfaces appear to be quite deep and the tip may not have fully probed the depth

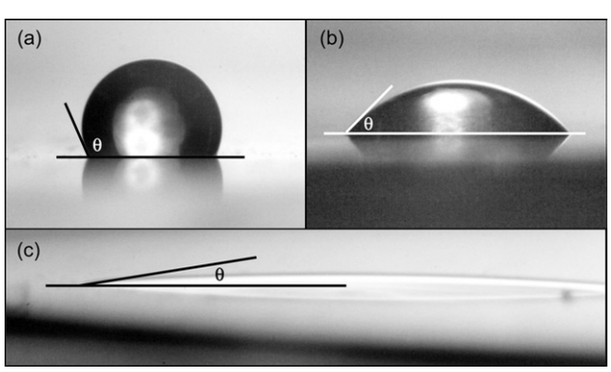

Fig. 3 Contact angle measurements of a 1 μL water droplet on three typical borosilicate glass surfaces: (a) halocarbon wax coated using the dip method, (b) untreated, and (c) plasma-cleaned.

Table 2 Summary of contact angle and AFM measurements.

Sample	Water contact angle/°	Surface roughness[a] average ± 1 *s*/Å
Hydrophilic samples		
Untreated glass	32 ± 2 (1 *s*)	10 ± 5
Water-rinsed glass	25	9 ± 3
Plasma-cleaned glass	<10	11 ± 2
H_2O_2-cleaned glass	<10	20 ± 1
Quartz	22 ± 4 (1 *s*)	62 ± 0.3
Hydrophobic samples		
Halocarbon wax: dip method	92	$> 145 \pm 13$[b]
Halocarbon wax: solvent method	83	> 24[b c]
Thin FEP Teflon film	109	$> 72 \pm 1$[b]
C8 SAM	98	9 ± 1
FEP Teflon film	102	(160 ± 24)[d]
PFA Teflon coating	112	(699 ± 18)[d]
Fluorofel PFC 801A coating	111	(126 ± 18)[d]

[a] Measured in non-contact mode on 5 μm × 5 μm sections. [b] Minimum value since AFM image (Fig. 5) suggests tip may not fully probe the minimum depth of the pores. [c] Much of the surface had what appeared to be particles embedded in the film, which could have been dust picked up during the coating. If these regions are included, the average roughness increases to 77 ± 76 Å. This is again a minimum value since the AFM tip may not fully probe the depth of pores. [d] Contact mode measurements made on 2 μm × 2 μm sections. Smaller surface roughness is typically measured in contact mode because topographic features that are associated with weakly adsorbed species such as water, surface structures, *etc.* are swept away by the tip which exerts appreciable force on the surface and thus wipes the surface as the image is being acquired.

of such pores. In addition, the values obtained depend on the particular portion of the surface scanned, and for irregular surfaces, this may vary from region to region. In general, as the size of the surface that is scanned increases, larger corrections for the low-frequency undulations of the surface are required. This increases the uncertainty of the RMS roughness value. As a result, these values can also be sensitive to the size of the area that is scanned. The average and standard deviation (1 *s*) values of surface roughness are summarized in Table 2, along with the areas used in each case.

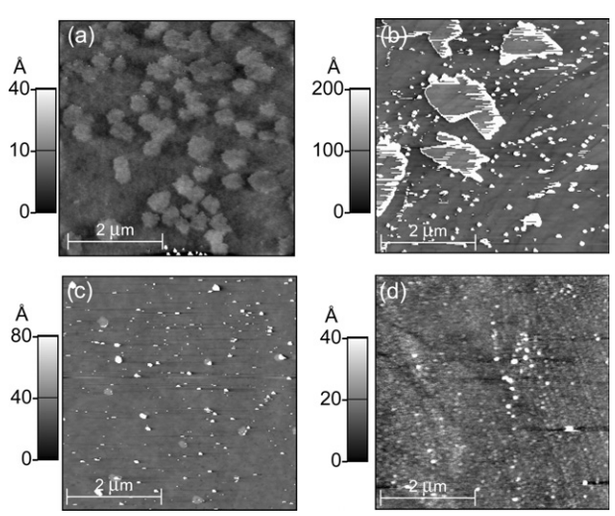

Fig. 4 AFM measurements (in non-contact mode) of the surface morphology for (a) untreated borosilicate glass; (b) untreated quartz; (c) borosilicate glass cleaned using hot H_2O_2; (d) borosilicate glass coated with the C8 SAM.

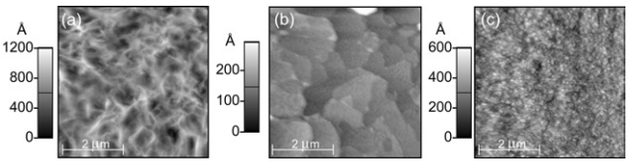

Fig. 5 AFM measurements (in non-contact mode) of the surface morphology for (a) borosilicate glass coated with halocarbon-wax using the dip method; (b) borosilicate glass coated using the solvent method and (c) FEP Teflon film.

C. Infrared measurements of water uptake

Fig. 6 shows typical infrared spectra for samples through which there was sufficient transmission of the infrared beam to make measurements of the weak absorptions due to water on the surface. The broad features from 2800–3800 cm^{-1} are due to OH stretching vibrations in condensed phase water.[40–44] The sharp peaks from 3500–3900 cm^{-1} are residuals due to subtraction of gas phase water. It has been shown that small thermal instabilities in the HeNe laser of the spectrometer, to which the absorption wavenumbers are referenced, can lead to shifts of up to ±0.034 cm^{-1} in the sharp rotational lines of gas phase water.[45] This made complete subtraction of the water impossible. However, this imperfect subtraction does not contribute significantly to the liquid water peak area since these sharp peaks are approximately equally positive and negative.

For comparison, the spectrum of bulk liquid water, obtained by placing a drop of water between two ZnSe windows, is also shown in Fig. 6-1a. At 80% RH, the peak positions and band shapes of water adsorbed on quartz, untreated glass, water-rinsed glass, and plasma-cleaned glass as well as the halocarbon wax coatings are similar to that of bulk liquid water. The peak on the H_2O_2 cleaned glass (Fig. 6-2d) is red-shifted significantly to ~3200 cm^{-1}. The C8 SAM and FEP Teflon film (Fig. 6-3i and 6-3j) take up much smaller amounts of

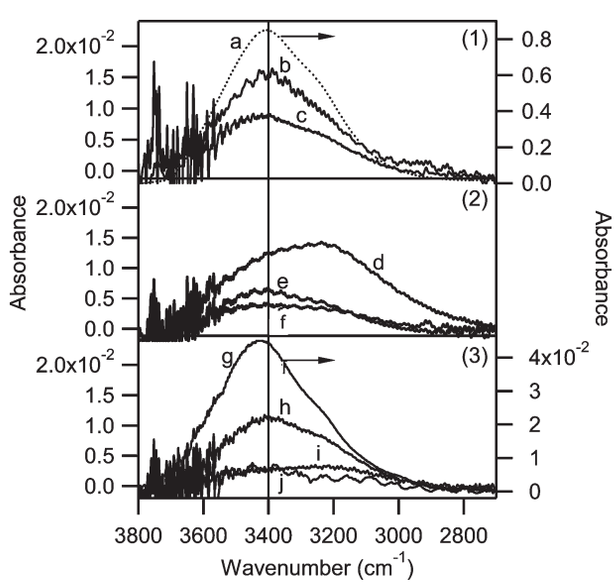

Fig. 6 Infrared spectra of surfaces in contact with N_2 at 80% RH and, for comparison, the spectrum of bulk liquid water: (1) bulk water (a, right axis), untreated glass (b), quartz (c); (2) H_2O_2 cleaned glass (d), plasma cleaned glass (e), and water rinsed glass (f); (3) dip method halocarbon wax (g, right axis), solvent method halocarbon wax (h), C_8 monolayer (i), and FEP Teflon film (j). The bulk water spectrum (1a) was obtained by measuring the IR transmission through a drop of water "sandwiched" between two ZnSe windows ratioed to the bare windows.

water; the peak for the water film on the C8 SAM is also red-shifted.

The liquid water peak can be used to estimate the number of water layers present on the surface as a function of relative humidity. The water coverage, Θ, in number of layers, is calculated from the absorbance spectra using eqn. (II), a modified form of Beer's law,[46]

$$\Theta = \frac{2.303A}{NS_{H_2O}\bar{\sigma}} \qquad \text{(II)}$$

where N is the number of surfaces in the infrared beam and S_{H_2O} is the surface density of one water monolayer (1.0×10^{15} molec cm^{-2}). The base-10 integrated absorbance, A, of the liquid water peak (from 2800 to 4000 cm^{-1}) is determined from the absorbance spectra. The integrated cross section, $\bar{\sigma}$ (to base e) was calculated for the same range to be 1.43×10^{-16} cm molecule^{-1} from optical constants reported by Downing and Williams.[47]

As shown in previous studies[1] and observed again in the present work (data not shown), the shape and peak position of the infrared spectrum of water on borosilicate glass change as the relative humidity is lowered. The peak becomes broader and shifts to higher wavenumbers. This is similar to observations of water uptake on other solids such as NaCl,[46,48,49] where the peak due to water condensed on the surface blue-shifts towards the gas phase absorption peak at low water coverages. This indicates disruptions in the 3-D hydrogen bonding network and strong interactions of the adsorbed water with the surface.[50,51] Similar results were observed in the present studies for water on plasma-cleaned glass, quartz, halocarbon wax, and Teflon film.

The absorption coefficients of water increase by approximately an order of magnitude from gas phase to bulk liquid water, and again from liquid to ice.[52,53] The true value of the integrated cross section for a structured, thin water film on a surface is likely to be different from the bulk water value and to vary with coverage. However, the island-like features in the AFM data (Fig. 4a) provide additional insight into the amount of liquid water present on glass, at least at RH above ~60%, and further analysis indicates that the estimate using the infrared absorption coefficient for liquid water is reasonable. Island-like features similar to those shown in Fig. 4a have been observed on surfaces such as mica in the presence of water vapor and have been attributed to islands of water on the surface.[54] The features in Fig. 4a are typically ~1.2 nm in height, corresponding to islands of water about three layers high. (The fraction of the surface covered with such islands was somewhat variable, likely reflecting variability in the relative humidity in the laboratory from day to day). The estimated number of layers of water using FTIR under similar conditions is 1.4, but this assumes an equal distribution of water over the surface. Given that AFM indicates that about half of the surface is covered with water islands, the amounts of water on the surface estimated using AFM and FTIR are consistent. To emphasize that the water measured using FTIR is not necessarily equally distributed over the surface, we express these data in terms of an ''equivalent number of water monolayers''.

For the H_2O_2-cleaned glass, there is a significant red-shift in the infrared peak at all relative humidities, in contrast to the other surfaces. Such a shift is characteristic of water with a more ice-like structure.[40–44] There may be shoulders on the low wavenumber side of the water peaks for plasma-cleaned glass, quartz and the solvent-coated halocarbon wax as well (Fig. 6).

Fig. 7 shows the equivalent number of water monolayers on the glass after various treatments, on quartz, and on halocarbon wax coatings prepared by different methods.

The results for water uptake on quartz are in excellent agreement with the previously reported results of Awakuni and Calderwood.[55] Fig. 7b shows data for two of the treated glass samples. (The isotherm for H_2O_2-cleaned glass is shown later.) Water coverage of these surfaces is similar to that of the untreated borosilicate glass up to approximately 60% RH, but is significantly smaller above 80% RH and does not show evidence of condensation as 100% RH is approached. Fig. 7c shows comparable data for the halocarbon wax coated surfaces. The halocarbon wax coating prepared by both the dip and solvent methods show evidence of multilayer adsorption similar to the untreated borosilicate glass.

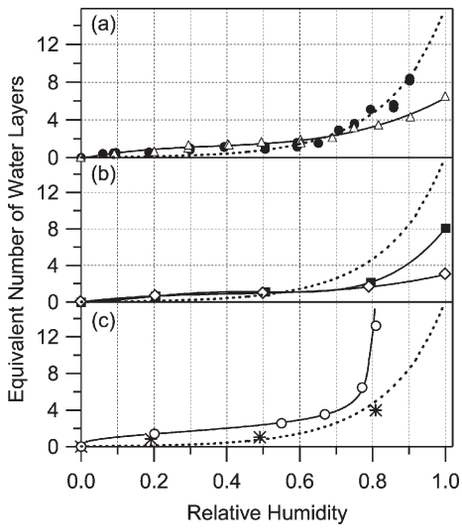

Fig. 7 Water uptake isotherms for (a) smooth untreated glass (solid circles) and quartz (open triangles); (b) water rinsed glass (open diamonds), and plasma cleaned glass (solid squares); and (c) dip method (open circles) and solvent method (asterisks) halocarbon wax coated glass. The dashed black line for the untreated borosilicate glass data in (a) is included in each panel as a guide for the eye. The solid lines are fits to each set of data, excluding the solvent method halocarbon wax, which falls on the fit for untreated glass. The dip method halocarbon wax data points (panel (c)) were taken after two hours equilibration time, although water uptake was still increasing for the high RH experiments (see text and Fig. 9).

As seen from the spectra in Fig. 6, the peak for the H_2O_2-treated glass is red-shifted quite substantially from that for bulk liquid water. This increases the uncertainty of the application of absorption coefficients for bulk, liquid water sufficiently that we chose not to estimate the number of monolayers using eqn. (II). However, one can examine the shape of the isotherm by using the measured absorbance of the band as a function of RH, as shown in Fig. 8 along with the isotherm for untreated glass. The dependence of the water uptake on RH is quite

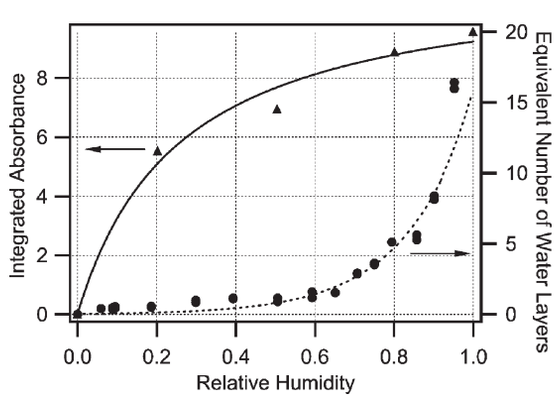

Fig. 8 Relative intensity of the liquid water peak, integrated from 2600–4000 cm^{-1}, on H_2O_2-cleaned borosilicate glass surface (triangles) as a function of relative humidity. The solid line is a fit to the data. Also shown for comparison is the isotherm for water uptake on untreated glass and the fit shown also in Fig. 7a as a guide.

different than for the untreated borosilicate glass, with the shape of water uptake on H_2O_2-treated glass resembling a Langmuir isotherm.[56–58]

While most surfaces came to equilibrium with water vapor within 15 minutes, the dipped halocarbon wax coating continued to take up water over more than an hour at higher relative humidities, as shown in Fig. 9. This is especially apparent at 81% RH, as water continued to adsorb to the surface even after 2 hours of exposure.

D. XPS analysis of surfaces

In order to assess the impact of the three cleaning methods applied to borosilicate glass, XPS measurements were made on the glass samples and, for comparison, the quartz sample. Fig. 10 shows the molar ratio of the major elements to the oxygen peak in each case. In the case of the quartz sample, the Si:O ratio is within experimental uncertainty of the expected SiO_2 stoichiometry. The more complex borosilicate glass samples show the expected large number of elements at the surface. As is common with surface analysis, there is always some adventitious carbon on the surfaces. However, clearly the H_2O_2 and plasma cleaning removed significant amounts of carbon from the surface.

As expected, quartz consists primarily of silica; small amounts of Na and Mg were also observed but may arise from contamination during sample handling and preparation. The borosilicate glass has substantial amounts of Na, B, K, and Zn. The surface of water-rinsed glass is similar in composition to that of untreated glass, with somewhat smaller Na. The increase in sodium for the plasma cleaned sample may result from the deposition of sodium from the inner chamber of the plasma cleaner, which is made of glass. Cleaning using H_2O_2 removes the B and K from the surface and substantially decreases the surface Zn and Na.

IV. Discussion

The goal of this work is to understand the interaction of water with various surfaces often used in laboratory studies of heterogeneous reactions that occur in thin water surface films at room temperature. As discussed in detail elsewhere,[5] rates of NO_2 hydrolysis calculated for experiments, such as that shown in Fig. 1, conducted in chambers of various sizes and wall composition can be compared after normalizing the rate for the surface-to-volume ratios of the reactors, the initial NO_2 concentrations, and the RH. Interestingly, the normalized rates of the heterogeneous hydrolysis of gaseous NO_2 that were measured in large smog chambers coated with hydrophobic Teflon[2,12] and in much smaller hydrophilic Pyrex cells[5]

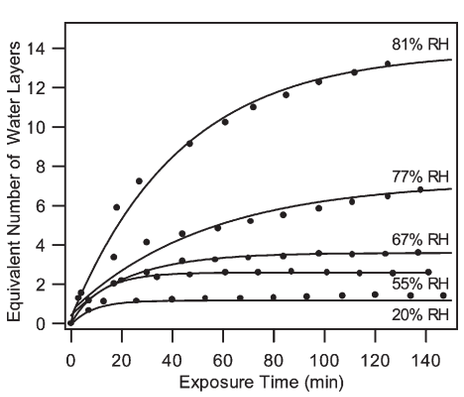

Fig. 9 Water uptake on halocarbon wax, (dip method) as a function of the exposure time to humidified nitrogen between 20% and 81% RH. The lines show exponential best fits to the data.

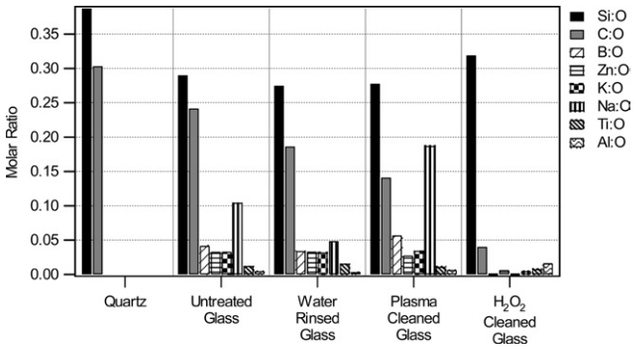

Fig. 10 XPS analysis of the surfaces of quartz, untreated borosilicate glass, borosilicate glass rinsed with Nanopure water, plasma-cleaned borosilicate glass, and H_2O_2-cleaned borosilicate glass. The molar ratios of various elements relative to oxygen are shown.

were similar. The data presented here provide some insights into why this is the case.

Borosilicate glass reactors are commonly used in many laboratory systems, and are known to adsorb water on their polar surface, which is terminated by Si–OH groups (*e.g.*, see refs. 1,59–62). The multilayer uptake of gases on solids is commonly described by the BET model, which predicts that the fractional coverage of the surface can be described by the BET eqn. (III),[56–58,62]

$$\text{fractional coverage} = \frac{c_B \text{RH}}{(1-\text{RH})[1+(c_B-1)\text{RH}]} \qquad \text{(III)}$$

where the constant $c_B \sim \exp\{(Q_1 - Q_v)/RT\}$ and Q_1 and Q_v are the enthalpy of adsorption of water on the substrate and on water itself (*i.e.* the enthalpy of condensation of water), respectively,[58] and RH represents the partial pressure of the adsorbate. The shape of the isotherm is therefore determined by the value of the constant c_B, which reflects the strength of the interaction of the gas with the substrate. Model BET isotherms are shown in Fig. 11 for c_B equal to 0.1 and 20. For c_B values larger than about 10, there is a ''knee'' in the isotherm at low RH; such isotherms are classified as Type II, and are typified by the uptake of water on polar surfaces.[62] For weak interactions between the gas and the surface, c_B is significantly smaller and the isotherms, classified as Type III, are smoothly concave with increasing relative humidity.[56–58,61,62] Type III isotherms are often observed for water on non-polar surfaces,[62] where it forms islands.[57] The AFM image in Fig. 4a does indeed show islands on the surface, which we attribute to water. While the AFM and infrared data are in reasonable agreement on the amount of water on the surface at relative humidities above ~60%, the smaller amounts of water at lower RH and the increased uncertainty in the appropriate infrared absorption coefficient in this region

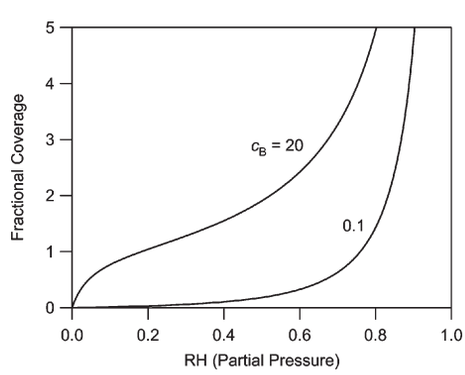

Fig. 11 Model Type II ($c_B = 20$) and Type III ($c_B = 0.1$) BET isotherms described by eqn. (III).

preclude definitively classifying the water uptake as Type II or Type III.

The BET isotherm (eqn. III) predicts that, as the vapor pressure of the adsorbate is approached, the number of adsorbed layers should approach infinity, *i.e.* the surface should become fully covered with liquid water. However, as seen in Fig. 3b, water on the untreated borosilicate glass has a finite contact angle so that a drop of the bulk liquid is present at the same time that there is a thin film of water on the surface. As discussed in detail by Adamson,[63] this situation is best described by Type VI and VII isotherms. On a molecular level, these isotherms occur in situations in which the structure of the adsorbate molecules closest to the surface is highly perturbed compared to the bulk liquid. A variety of evidence in the literature shows that water at the solid/water interface is structured and has properties different from bulk water; the structured orientation of surface water may extend anywhere from three monolayers to many molecular diameters.[50,64] It is also supported by the red-shift in the infrared spectrum of water adsorbed on borosilicate glass reported from earlier studies in this laboratory[1] and also observed in the present work.

The amount of adsorbed water on untreated glass in the present study is somewhat smaller than reported in earlier, preliminary studies in this laboratory.[1] This may be due to improved temperature control in the present experiments, variable degrees of organic contamination on the surfaces, or both. In any event, in typical laboratory glass vacuum systems, organic contamination from room air or backstreaming from pumps cannot be completely avoided and hence, the water uptake measured for the untreated borosilicate glass here should be comparable to that in such glass vacuum systems. It should be noted that surfaces in ambient air upon which heterogeneous chemistry occurs will also hold adsorbed organics.

The amount of water present on treated borosilicate glass shown in Fig. 7b demonstrates that the water uptake at higher RH is sensitive to the pretreatment of the surface, with less water uptake if the glass has been plasma-cleaned or even just rinsed with Nanopure water prior to the experiments. XPS analysis (Fig. 10) indicates that the inorganic surface composition of these samples is similar to that of the untreated glass. However, there is less carbon on the plasma-cleaned sample as expected, and perhaps on the water-rinsed glass. This suggests that some of the organic material on the untreated glass is comprised of oxidized, polar organics that can be removed by rinsing with water. Such polar organics may also help to adsorb water onto the surface. Although these samples show differences in sodium, the water-rinsed glass has less Na and the plasma-cleaned more than the untreated glass, there is no observed correlation between water uptake and the surface sodium. This is not surprising since there is also no obvious reason to expect sodium to be involved in water uptake. Derjaguin and Zorin[60] measured the thickness of water layers on cleaned smooth glass surfaces to be from a few Å to ~62 Å over the range from 95–100% RH; this would correspond to ~1–18 layers of water, consistent with the measurements reported here.

The H_2O_2-cleaned borosilicate glass is quite different from the other borosilicate glass samples in all of the characteristics studied here. The surface is now primarily composed of silica, with B, Zn, K and Na having been largely removed (Fig. 10), showing that the surface of the glass has been modified by the H_2O_2 treatment. The bulk most likely is not modified. The AFM image (Fig. 4c) does not show the islands of water seen on the untreated glass. The water uptake (Fig. 8) is similar to a Type I Langmuir adsorption isotherm for which there are a fixed number of surface sites that become saturated at high adsorbate gas concentrations, or alternatively, a microporous surface in which the pores become progressively filled with water.[56,58,62] The shift in the infrared absorption peak to ~3200 cm^{-1} suggests a more ice-like structure of the adsorbed water.[40–44] The combination of all of these data suggest that the H_2O_2 forms micropores on leaching the trace metals, and these provide the major sites for water uptake.

Perhaps most interesting is the interaction of water with halocarbon wax, Teflon and the C8 SAM. Although these materials are classically considered to be hydrophobic, which is supported by the large measured contact angles (Table 2), the water uptake measurements indicate that a significant amount of water, similar to that on untreated borosilicate glass, can be taken up on the halocarbon wax coated glass, and to a lesser extent, on the smooth FEP Teflon film and C8 SAM (Fig. 6). It is known that, on single crystal surfaces, water tends to adsorb at surface defects (*e.g.*refs. 65,66). Thus, adsorption of water onto solid surfaces may be dependent on the roughness of the surface, in addition to its chemical properties. For example, Rudich *et al.*,[67] showed that the corrugation of hydrophobic surfaces impacted the interaction with water and that more corrugated surfaces did, in fact, hold more water than the smooth organic films.

The AFM images support the hypothesis that surface roughness plays a major role in water uptake on the surfaces that are hydrophobic on a macroscopic scale. The halocarbon wax sample coated using the dip method is seen in Fig. 5a to have a very porous, web-like structure with deep and tortuous channels. The increased time to come to equilibrium with gas phase water (Fig. 9) is therefore not surprising. This highly irregular and porous surface leads to significant amounts of water uptake, indeed, more than that on the untreated borosilicate glass surface (Fig. 7c). The solvent-coated halocarbon wax (Fig. 5b) has less surface roughness and does not appear to be as porous, but is still much more irregular than the glass and quartz (Table 2 and Fig. 4) so that uptake on surface discontinuities may occur. As seen in Fig. 7, the water uptake on the solvent-coated halocarbon wax surface (Fig. 7c) is similar to that on the untreated borosilicate glass (Fig. 7a). It is possible that the halocarbon wax coatings also have some adsorbed polar organics that assist in water uptake.

The thin FEP Teflon film also takes up some water (Fig. 6c), estimated to be ~2 equivalent layers of water at 80% RH and rising to ~6 equivalent layers at 100% RH, significantly less than the halocarbon wax coatings. Awakuni and Calderwood[55] reported uptake of three layers of water by Teflon film at 100% RH. Svensson *et al.*[3] reported two layers on Teflon film at 5% relative humidity, with condensation on the surface at 90% RH; however, it is not clear that the surface structure of the material in those studies is comparable to the Teflon film used here. The AFM image of our Teflon film sample (Fig. 5c) shows very small pores that may be responsible for water uptake. The depth of these pores is greater on average than those in the C8 SAM, as indicated by a surface roughness of > 72 Å compared to 9 Å for the SAM. The smooth, relatively defect-free nature of the C8 SAM is likely responsible not only for the small amounts of water it takes up, but also for the shift in the infrared spectrum (Fig. 6c) to a more ice-like structure. The small amounts of water that are adsorbed on the C8 SAM may be taken up in defects in the coating which expose small regions of the underlying glass substrate, and/or on some of the elevated features on the surface seen in Fig. 4d.

As discussed earlier, laboratory studies of heterogeneous atmospheric reactions in thin aqueous films have typically used reactors made of glass, quartz, Teflon-coated glass or metal, and thin FEP Teflon films. The similarity in kinetics and mechanisms for the NO_2 heterogeneous hydrolysis in a halocarbon wax coated chamber (Fig. 1) to that in borosilicate glass chambers[5] can now be understood since the two surfaces have now been shown to adsorb similar amounts of water (Fig. 7c). Given the importance of surface structure (*e.g.* roughness and porosity) for water adsorption, it is expected that the FEP and PFA Teflon coatings, which also have quite high surface

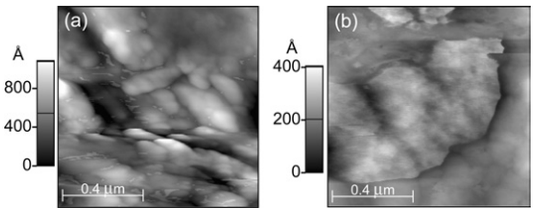

Fig. 12 AFM images of (a) a green ivy leaf surface with an RMS surface roughness of 195 Å and (b) a *Vinca minor* flower petal with an RMS surface roughness of 51 Å.

roughness values (Table 2), would behave in a similar manner to the halocarbon wax coatings. Thus, the agreement with studies carried out in Teflon-coated smog chambers[2,12] is also understandable.

Thin films of FEP Teflon adsorb substantially less water than the halocarbon wax, and presumably less than the similarly rough Teflon coatings as well. The much smaller water uptake on smooth FEP Teflon films is consistent with the smaller rates of NO_2 heterogeneous hydrolysis measured by Pitts *et al.*[2] and Svensson *et al.*[3] However, it should be noted that in experiments using chambers constructed of such films, other materials inside the chambers such as optics and sampling lines may contribute significantly to the uptake of water and hence the surface available for heterogeneous chemistry.

V. Atmospheric implications

As discussed in more detail elsewhere,[5,68] silicates are common components of many surfaces found in building materials, including concrete, asphalt, and window glass.[69] In addition, silica has been identified as a major component of soil and soil derived dust.[30,70] The uptake of water on such surfaces is known to promote heterogeneous chemistry not only in laboratory systems (*e.g.*, refs. 1,5) but also on surfaces found in the tropospheric boundary layer. Therefore, our measurements of water uptake on borosilicate glass and quartz are relevant and useful for understanding chemistry on these tropospheric surfaces.

Given our measurements showing that water adsorbs even to hydrophobic materials if their surfaces have appropriate roughness, it is likely that other hydrophobic materials, such as vegetation, may also hold water in quantities sufficient to support heterogeneous chemistry. Fig. 12 shows AFM images of the surfaces of an ivy leaf and a *Vinca minor* flower petal. Clearly there are surface irregularities that, despite the hydrophobic nature of the surfaces, should lead to water uptake in a manner similar to the halocarbon wax. The surface roughness values for a 1 $\mu m \times 1$ µm section of each sample were 195 Å for an ivy leaf and 51 Å for the *V. minor* petal, similar to the values for halocarbon wax and Teflon in Table 2. Water uptake on vegetation and its participation in heterogeneous reactions in the atmosphere is supported by the observation of HONO production over a variety of surface types, including vegetation.[19,23–30]

The results presented here give a strong indication that most, if not all, surfaces in contact with the atmosphere will hold water in sufficient amounts to promote heterogeneous reactions. Further field investigations of surface chemistry and elucidation of the impact of including heterogeneous reactions (*e.g.* reactions (1) and (2)) in atmospheric models are necessary to determine the full role played by heterogeneous chemistry in the atmosphere.

Acknowledgements

We are grateful to the California Air Resources Board (Contract No. 00-323) and the National Science Foundation (Grant No. CHE-0209719) for support of this work, and James N. Pitts Jr. for many stimulating discussions. RMP and EJM acknowledge funding from the National Science Foundation (Grant No. CHE-011155). We also thank Husheng Yang, Theresa McIntire, and Peter Griffiths for helpful discussions, James E. Rutledge and Justin Burton for their assistance in measurement of water contact angles, and Lisa Lucio Gough for assistance with manuscript preparation. We thank Paul Wennberg as well as Crest Coating and Livingstone Coating Corp. for providing the Teflon coated samples and Teflon film.

References

1 N. Saliba, H. Yang and B. J. Finlayson-Pitts, *J. Phys. Chem. A*, 2001, **105**, 10 339.
2 J. N. Pitts, Jr., E. Sanhueza, R. Atkinson, W. P. L. Carter, A. M. Winer, G. W. Harris and C. N. Plum, *Int. J. Chem. Kinet.*, 1984, **16**, 919.
3 R. Svensson, E. Ljungstrom and O. Lindqvist, *Atmos. Environ.*, 1987, **21**, 1529.
4 M. E. Jenkin, R. A. Cox and D. J. Williams, *Atmos. Environ.*, 1988, **22**, 487.
5 B. J. Finlayson-Pitts, L. M. Wingen, A. L. Sumner, D. Syomin and K. A. Ramazan, *Phys. Chem. Chem. Phys.*, 2003, **5**, 223.
6 L. G. Wayne and D. M. Yost, *J. Chem. Phys.*, 1951, **19**, 41.
7 J. Cathala and G. Weinrich, *Compt. Rend.*, 1952, **244**, 1502.
8 M. S. Peters and J. L. Holman, *Ind. Eng. Chem.*, 1955, **47**, 2536.
9 G. G. Goyer, *J. Colloid Sci.*, 1963, **18**, 616.
10 C. England and W. H. Corcoran, *Ind. Eng. Chem. Fundam.*, 1974, **13**, 373.
11 H. M. Ten Brink, J. A. Bontje, H. Spoelstra and J. F. van deVate, in *Studies in Environmental Science*, ed. M. M. Benarie, Elsevier, Amsterdam, 1978, vol. 1, pp. 239.
12 F. Sakamaki, S. Hatakeyama and H. Akimoto, *Int. J. Chem. Kinet.*, 1983, **15**, 1013.
13 H. Akimoto, H. Takagi and F. Sakamaki, *Int. J. Chem. Kinet.*, 1987, **19**, 539.
14 A. Febo and C. Perrino, *Atmos. Environ.*, 1991, **25A**, 1055.
15 A. Bambauer, B. Brantner, M. Paige and T. Novakov, *Atmos. Environ.*, 1994, **28**, 3225.
16 J. Kleffmann, K. H. Becker and P. Wiesen, *Atmos. Environ.*, 1998, **32**, 2721.
17 J. Kleffmann, K. H. Becker and P. Wiesen, *J. Chem. Soc., Faraday Trans.*, 1998, **94**, 3289.
18 R. M. Harrison and G. M. Collins, *J. Atmos. Chem.*, 1998, **30**, 397.
19 G. Lammel, *Formation of Nitrous Acid - Parameterisation and Comparison with Observations*, Max Planck Institute for Meteorology, Hamburg, 1999, Report No. 286, pp. 1–36.
20 R. Kurtenbach, K. H. Becker, J. A. G. Gomes, J. Kleffmann, J. C. Lörzer, M. Spittler, P. Wiesen, R. Ackermann, A. Geyer and U. Platt, *Atmos. Environ.*, 2001, **35**, 3385.
21 A. L. Goodman, G. M. Underwood and V. H. Grassian, *J. Phys. Chem. A.*, 1999, **103**, 7217.
22 W. S. Barney and B. J. Finlayson-Pitts, *J. Phys. Chem. A*, 2000, **104**, 171.
23 D. Perner and U. Platt, *Geophys. Res. Lett.*, 1979, **6**, 917.
24 U. Platt, D. Perner, G. W. Harris, A. M. Winer and J. N. Pitts, Jr., *Nature*, 1980, **285**, 312.
25 A. M. Winer and H. W. Biermann, *Res. Chem. Intermed.*, 1994, **20**, 423.
26 R. M. Harrison, J. D. Peak and G. M. Collins, *J. Geophys. Res*, 1996, **101**, 14 429.
27 G. Lammel and J. N. Cape, *Chem. Soc. Rev*, 1996, **25**, 361.
28 J. Stutz, B. Alicke and A. Neftel, *J. Geophys. Res*, 2002, **107**, 8192.
29 B. Alicke, U. Platt and J. Stutz, *J. Geophys. Res. Atmos.*, 2002, **107**, 8196.
30 B. J. Finlayson-Pitts and J. N. Pitts, Jr., *Chemistry of the Upper and Lower Atmosphere: Theory, Experiments and Applications*, Academic Press, San Diego, 2000.
31 D. O. DeHaan, T. Brauers, K. Oum, J. Stutz, T. Nordmeyer and B. J. Finlayson-Pitts, *Int. Rev. Phys. Chem.*, 1999, **18**, 343.
32 *Standard Specifications for Glasses in Laboratory Apparatus*, ASTM International, West Conshohocken, PA, 2001.
33 T. H. Elmer, in *Engineered Materials Handbook*, vol. 4, Ceramics and Glasses, ASM International, Materials Park, OH, 1992, vol. 4, pp. 427.
34 J. Sagiv, *J. Am. Chem. Soc.*, 1980, **102**, 92.

35 Graciously provided by Paul Wennberg.
36 A. Ulman, *An Introduction to Ultrathin Organic Films From Langmuir-Blodgett to Self Assembly*, Academic Press, San Diego, 1991.
37 P. R. Griffiths and J. A. de Haseth, *Fourier Transform Infrared Spectrometry*, Wiley, New York, 1986.
38 C. S. Hemminger, T. A. Land, A. Christie and J. C. Hemminger, *Surf. Interface Anal.*, 1990, **15**, 323.
39 C. D. Wagner, L. E. Davis, M. V. Zeller, J. A. Taylor, R. H. Raymond and L. H. Gale, *Surf. Interface Anal.*, 1981, **3**, 211.
40 G. Herzberg, *Molecular Spectra and Molecular Structure. II. Infrared and Raman Spectra of Polyatomic Molecules*, D. Van Nostrand Company, Inc., Princeton, N. J., 1945, vol. II.
41 Q. Du, E. Freysz and Y. R. Shen, *Phys. Rev. Lett.*, 1994, **72**, 238.
42 Q. Du, E. Freysz and Y. R. Shen, *Science*, 1994, **264**, 826.
43 M. J. Shultz, C. Schnitzer, D. Simonelli and S. Baldelli, *Int. Rev. Phys. Chem.*, 2000, **19**, 123.
44 G. L. Richmond, *Annu. Rev. Phys. Chem.*, 2001, **52**, 357.
45 D. D. Weis and G. E. Ewing, *Anal. Chem.*, 1998, **70**, 3175.
46 M. C. Foster and G. E. Ewing, *J. Chem. Phys*, 2000, **112**, 6817.
47 H. D. Downing and D. Williams, *J. Geophys. Res.*, 1975, **80**, 1656.
48 M. C. Foster and G. E. Ewing, *Surf. Sci*, 1999, **427–428**, 102.
49 W. Cantrell and G. E. Ewing, *J. Phys. Chem. B*, 2001, **105**, 5434.
50 W. Drost-Hansen, in *Chemistry and Physics of Interfaces*, American Chemical Society, Washington, DC, 1971, vol. 2, pp. 204.
51 *Adsorption on Silica Surfaces*, ed. E. Papirer, Marcel Dekker, New York, 2000.
52 G. C. Pimental and A. L. McClelland, *The Hydrogen Bond*, Reinhold, New York, 1960.
53 W. M. Irvine and J. B. Pollack, *Icarus*, 1968, **8**, 324.
54 L. Xu, A. Lio, J. Hu, D. F. Ogletree and M. Salmeron, *J. Phys. Chem. B*, 1998, **102**, 540.
55 Y. Awakuni and J. H. Calderwood, *J. Phys. D*, 1972, **5**, 1038.
56 A. W. Adamson, *Physical Chemistry of Surfaces*, John Wiley & Sons, New York, 5th edn., 1990.
57 R. I. Masel, *Principles of Adsorption and Reaction on Surfaces*, John Wiley & Sons, New York, 1996.
58 A. W. Adamson and A. P. Gast, *Physical Chemistry of Surfaces*, John Wiley & Sons, Inc., New York, 6th edn., 1997.
59 I. Langmuir, *J. Amer. Chem. Soc.*, 1918, **40**, 1361.
60 B. V. Derjaguin and Z. M. Zorin, *2nd Proc. Intern. Congr. Surface Activity (London)*, 1957, **2**, 145.
61 A. W. Adamson, *Physical Chemistry of Surfaces*, John Wiley & Sons, New York, 1967.
62 S. J. Gregg and K. S. W. Sing, *Adsorption, Surface Area and Porosity*, 2nd edn., Academic Press, London, 1982.
63 A. W. Adamson, *J. Colloid Interface Sci.*, 1968, **27**, 180.
64 G. A. Parks, *J. Geophys. Res*, 1984, **89**, 3997.
65 D. Dai, S. J. Peters and G. E. Ewing, *J. Phys. Chem*, 1995, **99**, 10 299.
66 R. C. Hoffman, M. Kaleuati and B. J. Finlayson-Pitts, *J. Phys. Chem. A.*, 2003, **107**, 7818.
67 Y. Rudich, I. Benjamin, R. Naaman, E. Thomas, S. Trakhtenberg and R. Ussyshkin, *J. Phys. Chem. A*, 2000, **104**, 5238.
68 A. Rivera-Figueroa, A. L. Sumner and B. J. Finlayson-Pitts, *Environ. Sci. Technol.*, 2002, **37**, 548.
69 R. M. E. Diamant, *The Chemistry of Building Materials*, Business Books Limited, London, 1970.
70 D. Gillette, *J. Exposure Anal. Environ. Epidemiol.*, 1997, **7**, 303.